Comparative Evaluation of Thermal Imagery of Landsat-8 and ASTER in the Delineation of Lithology in Jahazpur, Rajasthan, India

Gaurav Mishra (1), Himanshu Govil (1), Subhanil Guha (1), Monika (1), Mahesh Kumar Tripathi (1), Arjun Pratap Shahi (1)
[1] Department of Applied Geology, National Institute of Technology Raipur- 492010, Chhattisgarh, India
Email: mshgaurav04@gmail.com; hgovil.geo@nitrr.ac.in; subhanilguha@gmail.com; geniousmonika11@gmail.com; TRIPATHI.MAHESH1@gmail.com; arjunpratapshahi@gmail.com

KEY WORDS: land surface temperature, thermal infrared, hydrothermally altered minerals

ABSTRACT: This study analyses the comparative estimation of land surface temperature variation with lithology at Jahazpur, Rajasthan using Landsat-8 OLI/TIRS data and ASTER (Advanced Spaceborne Thermal Emission and Reflection Radiometer) TIR sensors. The thermal infrared sensor (TIRS) on board the Landsat 8 is a key instrument to acquire thermal infrared (TIR) data. The Landsat series sensors provide regularly acquired collection of space-based TIR data. The Advanced Spaceborne Thermal Emission and Reflection Radiometer (ASTER) onboard the Terra spacecraft continuously acquire Thermal Infrared (TIR) images with high spatial resolution. The satellite data in the TIR spectral band of Ladsat-8 OLI/TIRS (100m resolution, TIR) and ASTER (90m resolution, TIR data) used to map the land surface temperature. The land surface temperature affected by colour of rock which further depends on the mineralogical composition of the rock. Study area is composed of varied meta-sedimentary rock sequences affected by low grade greenschist facies of metamorphism. The dominant rock type includes phyllite, dolomite, orthoquartzite, dolomite with BIF, grey phyllite and gritty quartzite. The surface temperature estimated by Landsat-8 OLI/TIRS data and ASTER TIR data is compared with the lithological map, revealing the correspondence between LST of Landsat and ASTER with mineralogical composition of the area. The rocks such as gritty quartzite composed of brighter minerals (quartz) displays lower to intermediate temperature whereas dolomite with BIF shows intermediate to higher temperature. Spatial resolution greatly affects the image classification and finer spatial resolution decreases the effect of mixed pixel at boundary of a lithology. Therefore, the accuracy of ASTER data with 90m resolution was slightly higher than Landsat-8 OLI/TIRS data with 100m resolution in the delineation of surface lithology of the area based on land surface temperature maps.

1. Introduction

Remote sensing is the science of acquiring, processing and interpretation of images and related data acquired from aircraft and satellite which record the interaction between matter and electromagnetic energy (Sabins, 1999). It provides important information for exploration of minerals because of their variable spatial, radiometric and spectral resolution (Abdelkareem & El-Baz, 2018). Conventional geological mapping is the laborious, time-consuming and expansive work and require lot of man power and analytical processes. Identification and delineation of hydrothermal alteration zones and associated faults/fracture zone plays important role and key objective in the mineral exploration processes (Sabins, 1999; Cŕosta et al., 2003). Satellite remote

sensing have been successfully implied in association with geographic information system (GIS) for lithological mapping and associated ore mineralization (Abrams et al., 1983; Rowan & Mars, 2003; Pour & Hashim, 2011). Multispectral imaging such as Landsat-8 and Advanced Spaceborne Thermal Emission and Reflection Radiometer (ASTER) provide valuable information for ore mineral exploration (Ahmadirouhani et al., 2018; Sheikhrahimi et al., 2019).

Hydrothermal alteration processes produce physico-chemical changes in the rocks through which they circulate. When the hydrothermal fluid comes in contact with the wall rock, a number of chemical reactions have been taken place and processes of dissolution and precipitation produce new mineral assemblages. The nature and type of hydrothermal alteration depends upon pressure, temperature and chemistry of circulating fluid as well as nature and composition of the rocks through which the fluid circulates.

LST (Land surface temperature) is the of Earth's surface temperature where the heat and radiation from the sun are reflected, absorbed and refracted. Ground survey permit a more accurate Land Use Land Cover (LULC) classification, but they are time-consuming and expensive and thus remote sensing become preferred alternative for LULC classification. LST is the key factor for calculating the temperature of a particular location. Landsat 8 carries two sensors i.e. the Operational Land Imager (OLI) and the Thermal Infrared Sensor (TIRS). TIRS acquire thermal infrared images at a spatial resolution of 100m using two bands located in the atmospheric window between 10 and 12 μm.

In May, 2013 Landsat-8 Operational Land Imager (OLI) became available as well as Thermal Infrared Sensor (TIRS) imagery. The data consists of nine spectral bands with a spatial resolution of 30 meters for Band 1 to 7 and 9, and Band 8 (panchromatic) have 15 meters resolution. Thermal bands 10 and 11 provide more accurate land surface temperature with 100m spatial resolution.

The present study uses the Landsat 8 multispectral data acquired on 10 November 2018 with calm weather and 0% cloud cover. The imagery has been downloaded from USGS Earth Explorer.

The Advanced Spaceborne Thermal Emission and Reflection Radiometer (ASTER) have been developed in Japan and data is available for government, industry and research groups. The thermal infrared data have wavelength 8.125 and 11.65 micrometre and with a spatial resolution of 90m. The ASTER Level 1 Precision Terrain Corrected Registered At-Sensor Radiance (AST_L1T) data of 13 November 2018 have been downloaded from USGS Global Visualization Viewer (GloVis).

Present study provides comparative potential of ASTER and Landsat-8 thermal data in the delineation of lithology of the area. This will be achieved mainly by land surface temperature determination using Landsat-8 TIRS and ASTER thermal data spatial resolution 100m and 90m respectively.

2. Study area

The study area is located in Jahazpur town of Bhilwara district and 21 km north-west of Deoli in the state of Rajasthan, India. The NE-SW trending Jahazpur belt is linear shape and extend continuously pinching out at the end. It is subdivided into two linear belts namely Eastern Jahazpur belt and Western Jahazpur belt (Malhotra & Pandit, 2000). The eastern belt extends from Khorpur in the SW to Naenwa in NE and the Western belt extends from Jawal in SW to Dhandola in NE. The Western Jahazpur belt extend for 60 km and Eastern Jahazpur belt for 90 km and the width of these belts vary between 1 to 3 km (Sinha-roy, Malhotra, & Mohanty, 1998). Jahazpur belt is dominated by metasedimentary rocks which display low-grade greenschist facies of metamorphism. The primary rock type of the Jahazpur belt include phyllite, dolomite,

orthoquartzite, granite, conglomerate and gritty quartzite overlying on Archean basement. The rocks are affected by multiple deformation phases and evident by presence of folded strata.

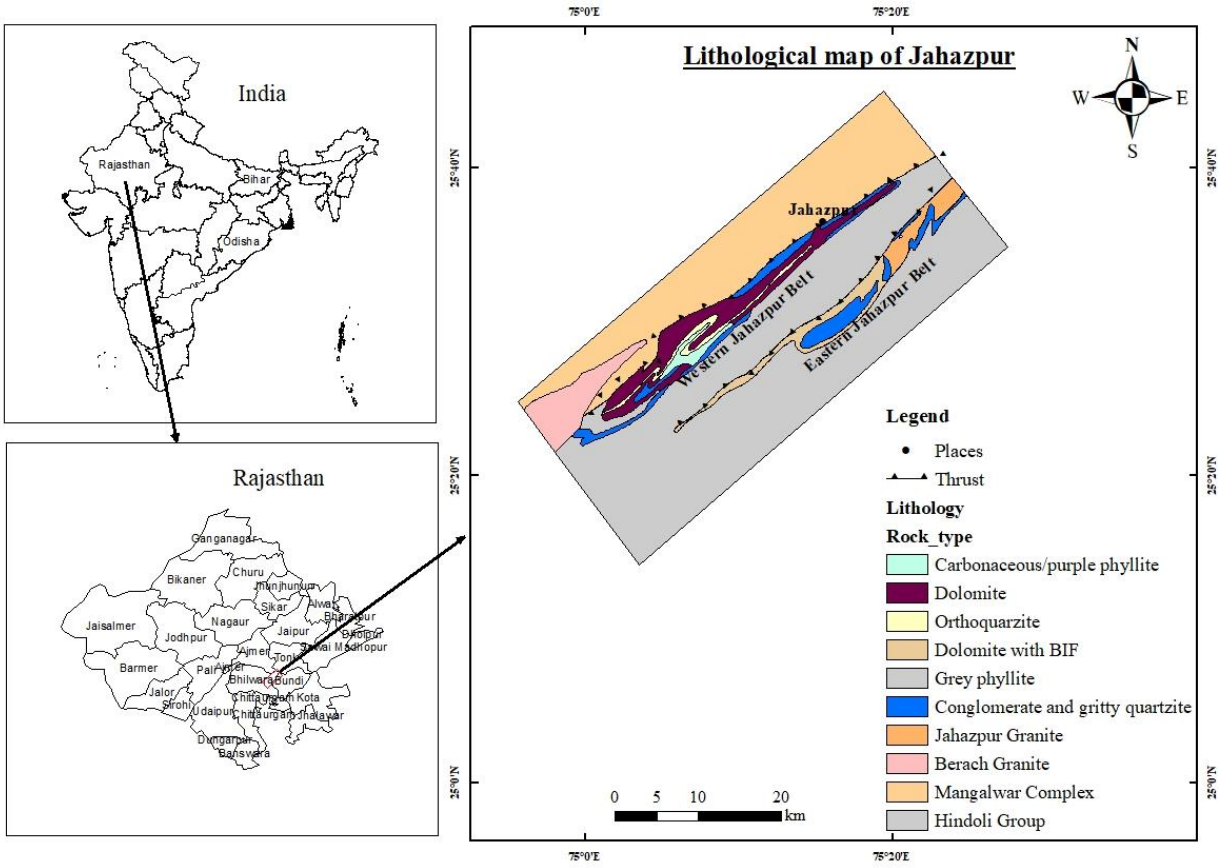

Figure 1. Geological map of the study area with different rock type of Jahazpur belt, Bhilwara district, Rajasthan (Modified after Pandit et al. 2003).

3. Materials and Methods

3.1 Data Used

3.1.1 Landsat-8 data

Landsat is the Landsat series of satellites and data is available is USGS (United States Geological Survey) Earth Explorer website. Landsat-8 satellite images the entire Earth once in 16 days. Landsat-9 TIR bands 10 and 11 were used to estimate brightness temperature and bands 4 and 5 were used to generate NDVI of the area. Bands, wavelength and Resolution of landsat-8 are given in the following Table 1:

Table 1. Characteristics of Landsat 8 OLI/TIRS sensors (Roy et al., 2014).

Bands	Wavelength (µm)	Resolution (m)
Band 1 - Ultra Blue (Coastal/Aerosol)	0.435 – 0.451	30
Band 2 – Blue	0.452 – 0.512	30
Band 3 – Green	0.533 – 0.590	30
Band 4 – Red	0.636 – 0.673	30
Band 5 – Near Infrared (NIR)	0.851 – 0.879	30
Band 6 – Shortwave Infrared (SWIR) 1	1.566 – 1.651	30
Band 7 – Shortwave Infrared (SWIR) 2	2.107 – 2.294	30
Band 8 – Panchromatic	0.503 – 0.676	15
Band 9 – Cirrus	1.363 – 1.384	30

Band 10 – Thermal Infrared (TIRS) 1	10.60 – 11.19	100
Band 11 – Thermal Infrared (TIRS) 2	11.50 – 12.51	100

Following Meta data values are used for calculation

- Radiance Add Band 10 = 0.10000
- Radiance Add Band 11 = 0.10000
- Radiance Mult Band 10 = 0.0003342
- Radiance Mult Band 11 = 0.0003342
- K1 Constant band 10 = 774.8853
- K2 Constant band 10 = 1321.0789
- K1 Constant band 11 = 480.8883
- K2 Constant band 11 = 1201.1442

3.1.2 ASTER data

The ASTER instrument scene consists of fourteen bands which can detect electromagnetic radiation ranging from the visible region to the thermal infrared region of the electromagnetic spectrum. The sensor was launched in 1999 and instrument was carried by National Aeronautics and Space Administration's (NASA) Terra spacecraft. For the present study band number 14 TIR (10.95-11.65 µm) was used for land surface determination. ASTER band, resolution and wavelength are shown in the following Table 2.

Table 2. Characteristics of ASTER bands, wavelength and resolution (Fujisada et al., 1998).

Electromagnetic Range	ASTER Bands	Wavelength (µm)	Resolution (m)
Visible and Near Infrared (VNIR)	Band 1 - Green	0.52 - 0.60	15
	Band 2 - Red	0.63 - 0.69	15
	Band 3N - Near Infrared (NIR)	0.78 - 0.86	15
Short Wave Infrared (SWIR)	Band 4 - SWIR 1	1.60 - 1.70	30
	Band 5 - SWIR 2	2.145 - 2.185	30
	Band 6 - SWIR 3	2.185 - 2.225	30
	Band 7 - SWIR 4	2.235 - 2.285	30
	Band 8 - SWIR 5	2.295 - 2.365	30
	Band 9 - SWIR 6	2.360 - 2.430	30
Thermal Infrared (TIR)	Band 10 - TIR 1	8.125 - 8.475	90
	Band 11 - TIR 2	8.475 - 8.825	90
	Band 12 - TIR 3	8.925 - 9.275	90
	Band 13 - TIR 4	10.25 - 10.95	90
	Band 14 - TIR 5	10.95 - 11.65	90

3.2 Process of LST determination

3.2.1 Landsat-8 data in determination of Land Surface temperature (LST)

i. Top of Atmosphere (TOA) Radiance:

Using the radiance rescaling factor, Thermal Infrared digital numbers can be converted to TOA spectral radiance.

$$L\lambda = (\text{ML} \times \text{Qcal}) + \text{AL}$$

Where:

Lλ = TOA spectral radiance (watt/m^{2}srμm)

ML = Radiance multiplicative band (no.)

AL = Radiance Add band (no.)

Qcal = Quantized and calibrated standard product pixel value (DN)

ii. Top of Atmosphere (TOA) brightness temperature

Spectral radiance data can be transformed into top of atmosphere brightness temperature using the thermal using the thermal constant values in data file.

$$BT = K2 \,/\, \ln\left(\frac{K1}{L\lambda} + 1\right) - 273.15$$

Where:

BT = top of atmosphere brightness temperature (°C)

Lλ = TOA spectral radiance (watt/m^{2}srμm)

K1 = K1 constant band (no.)

K2 = K2 constant band (no.)

iii. Normalized Differential Vegetation Index (NDVI):

The NDVI is a standard vegetation index and can be calculated by using Near Infrared (Band 5) and Red (band 4) bands.

$$NDVI = (NIR - Red)/\,(NIR + Red)$$

Where:

Red = DN values from the red band

NIR = DN values from Near-Infrared band

iv. Land Surface Emissivity (LSE):

LSE is the average emissivity of an element of the surface of the eath calculated from NDVI values

$$PV = [(NDVI - NDVImin)/(NDVImax + NDVImin)]\text{^}2$$

Where

PV = proportion of vegetation

NDVI = DN values from NDVI image

NDVI min = Minimum DN values from NDVI image

NDVI max = Maximum DN values from NDVI image

$$E = (0.004 \times PV) + 0.986$$

Where

E = Land surface emissivity

PV = proportion of vegetation

v. Land Surface Temperature (LST)

Land surface temperature (LST) is the radiative temperature which is calculated by using Top of atmosphere brightness temperature, wavelength of emitted radiance and land surface emissivity.

$$\boldsymbol{LST} = \left(\frac{\boldsymbol{BT}}{\mathbf{1}}\right) + \boldsymbol{W} \times \left(\frac{\boldsymbol{BT}}{\mathbf{14380}}\right) \times \mathbf{ln}\,(\boldsymbol{e})$$

Where

BT = top of atmosphere brightness temperature (°C)

W = wavelength of emitted radiance

E = Land surface Emissivity

3.2.2 ASTER data in determination of Land Surface temperature (LST)

The spatial resolution of the ASTER 1T product is 90m and used to generate data for the temperature emissivity separation (TES) algorithm used for determining the emissivity of land coverage values.

The ASTER L1T data products are retrieved from NASA Land Processes Distributed Active Archive Center (LP DAAC), USGS/Earth Resources Observation and Science (EROS) Center.

Land Surface Temperature can be calculated from At-Satellite Brightness Temperature TB as (Weng, Lu, & Schubring, 2004):

$$T = TB/[1 + \left(\lambda \times \frac{\mathrm{TB}}{\mathrm{c2}}\right) \times \ln\,(e)]$$

Where

λ = wavelength of emitted radiance

c2 = h × c/s = 1.4388×10^{-2} mK

h = Planck's constant = 6.626×10^{-34} Js

s = Boltzmann constant = 1.38×10^{-23} J/K

c = velocity of light = 3×10^{8} m/s

Emissivity values of various land cover types are provided in the following Table 3:

Table 3. Emissivity (e) values for various land cover classes.

Land surface	Emissivity (e)
Soil	0.928

Grass	0.982
Asphalt	0.942
Concrete	0.937

At-Satellite Brightness Temperature to Land Surface Temperature using above equation. The values of λ for ASTER bands are listed in the following Table 4:

Table 4. Band number, wavelength and spatial resolution of ASTER TIRS data.

Band Number	Band wavelength (μm)	Mid-value of Wavelength, λ (μm)	Spatial Resolution (m)
10	8.125 – 8.475	8.3	90
11	8.475 – 8.825	8.65	90
12	8.925- 9.275	9.1	90
13	10.25 – 10.95	10.6	90
14	10.95 – 11.65	11.3	90

Band 13 of ASTER image used in the calculation of Land surface temperature:

$$\boldsymbol{LST = [Band13\ /(1 + \left(10.6\ \times \left(\frac{Band13}{14388}\right)\right) \times \ln\ (e))] - 273.15}$$

4. Results

Land surface temperature (LST) determined by Landsat-8 TIRS data shows 35.94 °C as highest temperature and 22.37 °C as lowest temperature. Maximum region shows temperature around 27 to 30 °C. The minimum temperature is found in the area composed of quartzite which is composed more than 90% of quartz mineral. Quartz is the light colour mineral and resistant mineral to the physical and chemical weathering. The area composed of dolomite with BIF shows intermediate temperature because of intermixing of light and dark coloured minerals.

ASTER TIR data shows 39.56 °C as highest and 20.86 °C as lowest temperature. The minimum temperature corresponds to the quartzite and patches of highest temperature shows by Mangalwar complex is metamorphosed in amphibolite facies of metamorphism. The interface between Mangalwar complex and western Jahazpur belt is marked by presence of thrust and associated with high heat flow. The mining areas of talc shows lesser surface temperature in both ASTER and Landsat-8 derived surface temperature map as compared with adjacent areas because of surface exposure of light-coloured minerals.

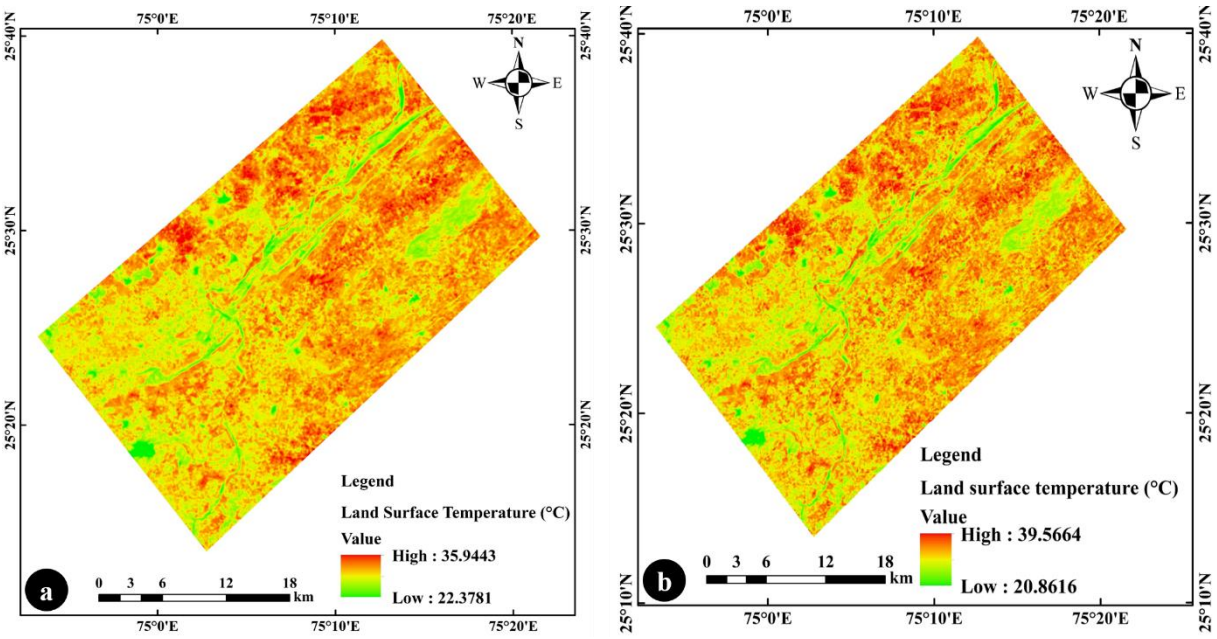

Figure 2. Land surface temperature map from a). Landsat 8 OLI/TIRS data; and b) ASTER TIRS data.

5. Conclusion

Lithologies on the basis of temperature can be outlined and corresponds to the lithological map of the area. The quartzite and dolomite rock unit are easily identified and delineated by both ASTER and Landsat-8 data. As the spatial resolution of Landsat-8 and ASTER TIR band is 100m and 90m respectively, the ASTER data found more useful in delineation of lithology whereas Landsat-8 data results in the mixing of pixels in the boundary of two adjacent lithologies.

References:

Abdelkareem, M., & El-Baz, F., 2018. Characterizing hydrothermal alteration zones in Hamama area in the central Eastern Desert of Egypt by remotely sensed data. Geocarto International, 33, pp. 1307–1325.

Abrams, M. J., Brown, D., Lepley, L., & Sadowski, R., 1983. Remote sensing for porphyry copper deposits in southern Arizona. Economic Geology, 78, pp. 591–604.

Ahmadirouhani, R., Karimpour, M.-H., Rahimi, B., Malekzadeh-Shafaroudi, A., Beiranvand Pour, A., & Pradhan, B. 2018. International Journal of Image and Data Fusion Integration of SPOT-5 and ASTER satellite data for structural tracing and hydrothermal alteration mineral mapping: implications for Cu-Au prospecting Integration of SPOT-5 and ASTER satellite data for structural tracing and hydrothermal alteration mineral mapping: implications for Cu-Au prospecting.

Cŕosta, A. P., De Souza Filho, C. R., Azevedo, F., & Brodie, C., 2003. Targeting key alteration minerals in epithermal deposits in Patagonia, Argentina, using ASTER imagery and principal component analysis. International Journal of Remote Sensing, 24, pp. 4233–4240.

Fujisada, H., Sakuma, F., Ono, A., & Kudoh, M., 1998. Design and preflight performance of aster instrument protoflight model. IEEE Transactions on Geoscience and Remote Sensing, 36, pp. 1152–1160.

Malhotra, G., & Pandit, M. K., 2000. Geology and mineralization of the Jahazpur Belt, southeastern Rajasthan. Narosa Publishing.

Pandit, M. K., Sial, A. N., Malhotra, G., Shekhawat, L. S., & Ferreira, V. P., 2003. C-, O-isotope and whole-rock geochemistry of proterozoic Jahazpur carbonates, NW Indian Craton. Gondwana Research, 6, pp. 513–522.

Pour, A. B., & Hashim, M., 2011. Identification of hydrothermal alteration minerals for exploring of porphyry copper deposit using ASTER data, SE Iran. Journal of Asian Earth Sciences, 42, pp. 1309–1323.

Rowan, L. C., & Mars, J. C., 2003. Lithologic mapping in the Mountain Pass, California area using Advanced Spaceborne Thermal Emission and Reflection Radiometer (ASTER) data. Remote Sensing of Environment, 84, pp. 350–366.

Roy, D. P., Wulder, M. A., Loveland, T. R., C.E., W., Allen, R. G., Anderson, M. C., Helder, D., Irons, J. R., Johnson, D. M., Kennedy, R., Scambos, T. A., Schaaf, C. B., Schott, J. R., Sheng, Y., Vermote, E. F., Belward, A. S., Bindschadler, R., Cohen, W. B., Gao, F., Hipple, J. D., Hostert, P., Huntington, J., Justice, C. O., Kilic, A., Kovalskyy, V., Lee, Z. P., Lymburner, L., Masek, J. G., McCorkel, J., Shuai, Y., Trezza, R., Vogelmann, J., Wynne, R. H., & Zhu, Z., 2014. Landsat-8: Science and product vision for terrestrial global change research. Remote Sensing of Environment, 145, pp. 154–172.

Sabins, F. F., 1999. Remote sensing for mineral exploration. Ore Geology Reviews, 14, pp. 157–183.

Sheikhrahimi, A., Pour, A. B., Pradhan, B., & Zoheir, B., 2019. Mapping hydrothermal alteration zones and lineaments associated with orogenic gold mineralization using ASTER data: A case study from the Sanandaj-Sirjan Zone, Iran. Advances in Space Research, 63, pp. 3315–3332.

Sinha-roy, S., Malhotra, G., & Mohanty, M., 1998. Geology of Rajasthan Geol. Soc. India.

Weng, Q., Lu, D., & Schubring, J., 2004. Estimation of land surface temperature-vegetation abundance relationship for urban heat island studies. Remote Sensing of Environment.